Title

f-Orbital Mixing in the Octahedral f2 Compounds UX6 2— [X = F, Br, Cl, I] and PrCl6 3—

Journal

The Journal of Physical Chemistry A, 124(21)

ISSN

1089-5639

Authors

Edelstein, Norman M

Lukens, Wayne W

Publication Date

2020-05-28

DOI

10.1021/acs.jpca.0c02022

Peer reviewed

f-Orbital Mixing in the Octahedral f^2 Compounds UX_6^{2-} [X = F, Br, Cl, I] and $PrCl_6^{3-}$

Norman M. Edelstein[1,*], Wayne W. Lukens[1,*]

[1]Chemical Sciences Division

Lawrence Berkeley National Laboratory

1 Cyclotron Rd.

Berkeley, CA 94720

*nmedelstein@lbl.gov, wwlukens@lbl.gov

Abstract

Understanding how interactions between the f-orbitals and ligand orbitals in lanthanide and actinide systems affect their physical properties is the central issue in f-element chemistry. A wide variety of approaches including both theoretical and experimental tools have been used to study these relationships. Among the most widely used tools has been crystal field theory (CFT), which bridges theory and experiment in that it is a model based largely on atomic theory that is parameterized using experimental data. Crystal field theory is quite accurate for the lanthanides, due in part to the highly contracted nature of the 4f-orbitals. For actinides, crystal field theory is less accurate, potentially due to the treatment of orbital mixing. In CFT, orbital mixing is handled implicitly by allowing the electron repulsion parameters (Slater F^k parameters) and the spin-orbit coupling constant to vary. As a result, orbital mixing in CFT is isotropic in that the F^k parameters and the spin-orbit coupling constant affect all f-orbitals equally. This approximation works well for the lanthanides due to the limited degree of orbital mixing in these complexes. In

actinide complexes, the 5f-orbitals have greater overlap with the ligand orbitals, and this approximation is less accurate than in the lanthanides. Here, we report a modification of CFT that includes the effect of orbital mixing on electron repulsion and spin-orbit coupling for each f-orbital. The model is applied to the tetravalent uranium hexahalide dianions and $PrCl_6^{3-}$ for which the energies of many low-lying excited states are known. The new model generally fits the data as well the traditional CFT although with fewer parameters. However, the new model does not fit the data better than the more complex CFT models of Faucher and coworkers. The results of the model show in detail how changes in overlap and orbital energies influence the energies of the bonding and antibonding orbitals.

Introduction

The role of f-orbitals in bonding has been the subject of numerous experimental and theoretical investigations. Initial crystal field models described the interactions between the ligands and f-orbitals as purely electrostatic;[1, 2] however, later work determined that the impact of the ligands on the energies of the f-orbitals was due to in large part to overlap (orbital mixing).[3-5] The crystal field model includes the effects of orbital mixing primarily by allowing the spin-orbit coupling constant, ζ, and the electron repulsion (Slater) parameters, F^ks (k = 2, 4, 6), to vary, thus reflecting the decreased f-orbital character caused by orbital mixing. Allowing ζ and F^ks to vary in this manner accounts for orbital mixing in an isotropic manner in that these changes affect all orbitals whether or not they are involved in bonding. The anisotropic impact of overlap between ligand orbitals and a specific f-orbital has also been accounted for, most notably by Stevens, who quantified the effect of orbital mixing on orbital angular momentum using the orbital reduction factor, k, which provides an anisotropic correction to the angular momentum operator, $\boldsymbol{l}$.[6] A fully

anisotropic model of orbital mixing, essentially a ligand field model for f elements, has been proposed by Judd, but has never been implemented to our knowledge.[7] Our contribution has been to introduce a refined molecular orbital (MO) model, based on the work of Thornley,[8] to a number of octahedral $5f^1$ complexes with halide, alkyl, alkoxide, amide, and ketimide ligands to better analyze the role of the 5f-orbitals in these f^1 systems.[9] This model is essentially a refinement of the earlier model used by Eisenstein and Pryce to describe the bonding in NpF_6.[10] In our model, the amount of orbital mixing involving the f-orbitals is used to decrease both the orbital angular momenta and the spin-orbit coupling constants of the singly occupied states. However, optical data for $5f^1$ octahedral systems are rather limited. In the work reported here, we apply an MO model to the $5f^2$ states in octahedral U^{4+} hexahalide complexes, and for comparison purposes, $4f^2$ $[PrCl_6]^{3-}$.[11-13] Optical spectra of these systems have been widely studied, and assignments for most of the 40 unique levels expected for two equivalent f-electrons in octahedral symmetry are quite extensive. Relative to the simple model used for f^1 systems, applying our model to f^2 systems requires quantifying how orbital mixing affects electron-electron repulsion.

The initial analyses of the optical spectra of the octahedral molecular ions of the tetravalent actinide ion U^{4+} were initiated and carried out by Satten and coworkers over a span of some twenty years.[14-18] Further data on these systems were obtained by Flint and Tanner and later by Tanner and others.[19-22] Over the years, these data have been analyzed using the parameterized Hamiltonian applied so successfully by the Crosswhites, Judd, and Carnall to the spectra of the trivalent actinide ions.[23-26] However for the U^{4+} complexes, the agreement between the parametric theory and the experimental levels was poorer (σ = 182 cm^{-1} for UCl_6^{2-}) than the

agreement for the trivalent actinide ions in the $LaCl_3$ host (σ = 19 cm^{-1} for U^{3+} in $LaCl_3$), where $\sigma = \Sigma[(\Delta i)^2/(n - p)]^{1/2}$, Δi is the difference between the observed and calculated energies, n is the number of excited states included in the fit, and p is the number of parameters varied. Faucher, Moune, Garcia, and Tanner were able to greatly improve the fit between experiment and theory for the assigned energy levels of U^{4+} in Cs_2UBr_6 and Cs_2ZrBr_6 by introducing into the parametric Hamiltonian a configuration interaction between the ground configuration, $5f^2$, and the $5f^17p^1$ configuration.[11] This additional perturbation reduced the mean deviation of 35 assigned levels from 246 cm^{-1} to 54 cm^{-1} with the addition of 5 more variable parameters. Subsequently in the analysis of the lanthanide complexes $[ErCl_6]^{3-}$ (Er^{3+} $4f^{11}$) and $[TmCl_6]^{3-}$ (Tm^{3+} $4f^{12}$), Faucher and coworkers determined that the numerical procedure was valid, but the configuration interaction was between $4f^n$ and the ligand to metal charge transfer state, $4f^{n+1}3p^5$, where a ligand electron has been promoted into the 4f-orbitals from the filled shell of one of the surrounding ligand Cl^- ions.[12, 27] Presumably then, for the $[UBr_6]^{2-}$ spectra, the perturbing configuration would then be $5f^33p^5$. As shown by Hubbard and coworkers, such a configuration interaction between a ligand to metal charge transfer state and the ground state is analogous to mixing between the metal and ligand orbitals in an MO model.[28]

Wagner, et al. reported and assigned the optical spectra of $[(C_2H_5)_4N]_2UF_6$ and $[(C_2H_5)_4N]_2UI_6$ at 77 K.[29] For the iodide compound, the spectrum is very similar to spectra of the bromide and chloride compounds. Assignments were made on the basis of assignments of the vibronic bands, which were both higher and lower in energy than the zero phonon transition. From these assignments, the zero phonon electronic transitions were deduced. A similar procedure was utilized for the fluoride data, but these assignments were more tentative as it was assumed that

the ordering of the electronic energy levels would be the same as for the heavier halide crystals. Barandiaran and Seijo[30, 31] have performed *ab initio* calculations for the energy levels of the U^{4+} ion diluted in Cs_2ZrCl_6 and in Cs_2GeF_6. In both crystals, U^{4+} ion is much larger than the M^{4+} ion of the host crystal. However, sufficient space is available in these hosts for the local coordination sphere to expand without affecting the overall local structure. For each system, they calculated the energy levels of the $5f^2$ configuration and compared their calculations with available experimental data. For the Cs_2ZrCl_6 host, extensive data is available, but for the fluoride host, the only reported data was the earlier study by Wagner, et al.[29] The experimental results of Wagner, et al. agree qualitatively with the calculated spectrum of Ordejon, et al.[31] in that the assigned peaks shift to higher energies, and the $5f^2$ energy range increases going from the chloride to the fluoride host.[31]

More recently, bonding in UX_6^{2-} has received additional experimental and computational attention. Notably, Minasian, et al. determined the extent of Cl 3p orbital mixing in MCl_6^{2-}, where M = Ti, Zr, Hf, and U.[32] This study was extended to the include the Np and Pu complexes by Su, et al.[33] Bonding in the uranium hexachlorides has been studied computationally as a function of oxidation state by Beekmeyer and Kerridge, who find that higher oxidation states lead to increased orbital mixing.[34] Finally, Jung, et al., have used wave function methods to study the bonding across a very wide series of halide complexes, MCl_6^{n-}, where M = Ce to Yb and Th to No, and n is 2 or 3.[35] This study determined the splitting of the f-orbitals using the ligand field parameters to gain a more detailed understanding of how bonding changes as one progresses along the lanthanide and actinide series and when the oxidation state changes. Stronger orbital mixing is observed early in both series and for metal complexes in higher oxidation states.

Judd has discussed the general problem of developing a ligand field theory for actinides.[7] The primary approximation is that the antibonding 5f wave function, ψ_t, may be expressed as $\psi_t = k_t f_t + \lambda_t \chi_t$, where f_t is the unperturbed, atomic 5f-orbital, χ_t is a superposition of ligand wave functions, and k_t and λ_t are the coefficients for the contributions from the 5f and ligand wave functions, respectively. Judd noted the crucial assumption is that all matrix elements involving the ligand wave functions are negligibly small and discussed the justification for this assumption.

We have approached the analysis of the optical data of two equivalent f-electrons in an octahedral crystal field by extending the one f-electron MO model used previously for the analysis of octahedral or pseudo-octahedral U^{5+} complexes,[9] which is a modified version of that presented by Thornley for Yb^{3+} complexes. To extend this model to f^2 complexes, we calculate the matrix elements for two equivalent f-electrons, as outlined by Eisenstein and Pryce[36] and later utilized by Edelstein,[37] in the $m_s^{(1)}$, $m_l^{(1)}$, $m_s^{(2)}$, $m_l^{(2)}$ basis set where m_s and m_l are the spin and orbital angular momentum quantum numbers and the superscripts $^{(1)}$ and $^{(2)}$ refer to electron 1 and electron 2, respectively. In our approach, we begin with the spin-orbit coupling constant, ζ, and the values of the electron repulsion parameters, F^ks, that were previously determined for U^{4+} and Pr^{3+} free ions in gas phase. To account for changes in electron repulsion between the two electrons due to orbital mixing, the free ion matrix elements are multiplied by the f-orbital coefficient in the corresponding MOs. Similarly, the free-ion, spin-orbit coupling matrix elements are also multiplied by the f-orbital coefficients of the MOs. In this way, we can model the mixing of the f-orbitals and ligand orbitals using the usual CF model as described below. This approach is largely based on the Judd's crucial assumption that the contribution of the

ligand wave function to matrix elements for the antibonding f-orbitals is negligible. An analogous approach was previously used by Lohr to analyze the effect of bonding on the electronic structures of high spin Mn^{2+} complexes.[38]

This report outlines the development of this model and applies it to explore the bonding in the title complexes. Using these results along with the estimated energies of the orbitals involved in bonding, we explore the origins of the destabilization of the f-orbitals and stabilization of the ligand orbitals using second order perturbation theory. We find that the destabilization of the f-orbitals is largely a function of the ligand orbital energies, with more strongly stabilized ligand orbitals producing a greater splitting of the f-orbitals. On the other hand, the stabilization of the ligand orbitals depends on both orbital overlap (overlap driven orbital mixing) and the relative energies of the metal and ligand orbitals (orbital energy degeneracy driven orbital mixing).

Theory

Crystal field Hamiltonian and wave functions for two f-electrons in octahedral symmetry in the $m_s^{(1)}$, $m_l^{(1)}$, $m_s^{(2)}$, $m_l^{(2)}$ basis

The Hamiltonian that we use for two f-electrons in octahedral symmetry consists of contributions from the crystal field, electron repulsion, and spin-orbit coupling, $H = H_{CF} + H_{ee} + H_{SO}$. We will address these contributions in turn. The crystal field Hamiltonian for a single f-electron in octahedral symmetry in given by eq 1 where B_0^4 and B_0^6 are the crystal field parameters, which describe the energies of the f-orbitals. The C_q^k tensor operators depend only on the angular coordinates and are readily evaluated.

$$H_{CF} = B_0^4\left[C_0^4 + \sqrt{5/14}\left(C_4^4 + C_{-4}^4\right)\right] + B_0^6\left[C_0^6 - \sqrt{7/2}\left(C_4^6 + C_{-4}^6\right)\right] \quad (1)$$

There are a number of different conventions for defining the crystal field parameters. The above equation uses the Wybourne convention.[39] An octahedral crystal field, O_h, splits the f-orbitals into orbitals with t_{1u}, t_{2u}, and a_{2u} symmetry. These crystal field levels are given in Figure 1.

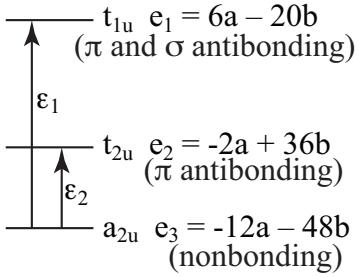

Figure 1: Splitting of the f-orbitals in an octahedral crystal field. a = $B_0^4/33$, b = (-5/429) B_0^6.

Judd[40] has given the energy levels and one-electron wave functions for the f-orbitals subject only to an octahedral crystal field in the m_l notation (m_l = -3, -2,…,+2, +3) as shown in Figure 1. He then included spin ($m_s = \pm 1/2$) to construct the one-electron wave functions for the f^1 system. These one-electron wave functions, given in Table 1, consist of two Γ_7 doublets (Γ_7 and $\Gamma_{7'}$), two Γ_8 quartets (Γ_8 and $\Gamma_{8'}$), and a single Γ_6 doublet.

Table 1 – The 14 wave functions for a single f-electron in an O_h crystal field (Judd, ref [40]).

Orbital symmetry	f^l state in Bethe notation	Wave function in $\|m_l, m_s\rangle$ notation $\|m_l = 0, m_s = -1/2\rangle$ is shown as $\|0-\rangle$
t_{1u}	Γ_{6-1}	$\sqrt{1/3}\,\|0-\rangle + \sqrt{5/12}\,\|3+\rangle + (1/2)\,\|-1+\rangle$
	Γ_{6-2}	$\sqrt{1/3}\,\|0+\rangle + \sqrt{5/12}\,\|-3-\rangle + (1/2)\,\|1-\rangle$
	$\Gamma_{8'-1}$	$\sqrt{2/3}\,\|0-\rangle - \sqrt{5/24}\,\|3+\rangle - \sqrt{1/8}\,\|-1+\rangle$
	$\Gamma_{8'-2}$	$\sqrt{2/3}\,\|0+\rangle - \sqrt{5/24}\,\|-3-\rangle - \sqrt{1/8}\,\|1-\rangle$
	$\Gamma_{8'-3}$	$\sqrt{5/8}\,\|3-\rangle + \sqrt{3/8}\,\|-1-\rangle$
	$\Gamma_{8'-4}$	$\sqrt{5/8}\,\|-3+\rangle + \sqrt{3/8}\,\|1+\rangle$
t_{2u}	$\Gamma_{7'-1}$	$\sqrt{1/6}\,\|2-\rangle + \sqrt{1/6}\,\|-2-\rangle + (1/2)\,\|-3+\rangle - \sqrt{5/12}\,\|1+\rangle$
	$\Gamma_{7'-2}$	$\sqrt{1/6}\,\|2+\rangle + \sqrt{1/6}\,\|2+\rangle + (1/2)\,\|3-\rangle - \sqrt{5/12}\,\|-1-\rangle$
	Γ_{8-1}	$\sqrt{1/3}\,\|2-\rangle + \sqrt{1/3}\,\|-2-\rangle - \sqrt{1/8}\,\|3+\rangle + \sqrt{5/24}\,\|1+\rangle$
	Γ_{8-2}	$\sqrt{1/3}\,\|2+\rangle + \sqrt{1/3}\,\|-2+\rangle - \sqrt{1/8}\,\|3-\rangle + \sqrt{5/24}\,\|-1-\rangle$
	Γ_{8-3}	$\sqrt{3/8}\,\|-3-\rangle - \sqrt{5/8}\,\|1-\rangle$
	Γ_{8-4}	$\sqrt{3/8}\,\|3+\rangle - \sqrt{5/8}\,\|-1+\rangle$
a_{2u}	Γ_{7-1}	$\sqrt{1/2}\,\|2-\rangle - \sqrt{1/2}\,\|-2-\rangle$
	Γ_{7-2}	$\sqrt{1/2}\,\|2+\rangle - \sqrt{1/2}\,\|-2+\rangle$

These 14 one-electron wave functions may be combined to form two-electron wave functions. We start with the $\Gamma_{7\text{-}1}$ wave function. To obey the Pauli principle, the second electron is added using a different one-electron wave function. We continue with this procedure to form a total of 91 two-electron wave functions. Table 2 lists the 91 two-electron wave functions formed from the one electron states using the nomenclature of Table 1. This rank is of course the same as for two equivalent f-electrons using the L S J m_J basis. In the $m_s^{(1)}$, $m_l^{(1)}$, $m_s^{(2)}$, $m_l^{(2)}$ basis, H_{CF} is diagonal, and the diagonal matrix elements depend only on the destabilization of the ligand orbitals. The off-diagonal matrix elements are related to H_{ee} and $H_{SO.}$

Table 2. The 91 two-electron wave functions utilizing the one-electron wave functions in Table 1

1 $\Gamma_{7\text{-}1}, \Gamma_{7\text{-}2}$	20 $\Gamma_{7\text{-}2}, \Gamma_{6\text{-}1}$	39 $\Gamma_{7'\text{-}2}, \Gamma_{8\text{-}3}$	58 $\Gamma_{8\text{-}2}, \Gamma_{6\text{-}1}$	77 $\Gamma_{6\text{-}1}, \Gamma_{6\text{-}2}$
2 $\Gamma_{7\text{-}1}, \Gamma_{7'\text{-}1}$	21 $\Gamma_{7\text{-}2}, \Gamma_{6\text{-}2}$	40 $\Gamma_{7'\text{-}2}, \Gamma_{8\text{-}4}$	59 $\Gamma_{8\text{-}2}, \Gamma_{6\text{-}2}$	78 $\Gamma_{6\text{-}1}, \Gamma_{8'\text{-}1}$
3 $\Gamma_{7\text{-}1}, \Gamma_{7'\text{-}2}$	22 $\Gamma_{7\text{-}2}, \Gamma_{8'\text{-}1}$	41 $\Gamma_{7'\text{-}2}, \Gamma_{6\text{-}1}$	60 $\Gamma_{8\text{-}2}, \Gamma_{8'\text{-}1}$	79 $\Gamma_{6\text{-}1}, \Gamma_{8'\text{-}2}$
4 $\Gamma_{7\text{-}1}, \Gamma_{8\text{-}1}$	23 $\Gamma_{7\text{-}2}, \Gamma_{8'\text{-}2}$	42 $\Gamma_{7'\text{-}2}, \Gamma_{6\text{-}2}$	61 $\Gamma_{8\text{-}2}, \Gamma_{8'\text{-}2}$	80 $\Gamma_{6\text{-}1}, \Gamma_{8'\text{-}3}$
5 $\Gamma_{7\text{-}1}, \Gamma_{8\text{-}2}$	24 $\Gamma_{7\text{-}2}, \Gamma_{8'\text{-}3}$	43 $\Gamma_{7'\text{-}2}, \Gamma_{8'\text{-}1}$	62 $\Gamma_{8\text{-}2}, \Gamma_{8'\text{-}3}$	81 $\Gamma_{6\text{-}1}, \Gamma_{8'\text{-}4}$
6 $\Gamma_{7\text{-}1}, \Gamma_{8\text{-}3}$	25 $\Gamma_{7\text{-}2}, \Gamma_{8'\text{-}4}$	44 $\Gamma_{7'\text{-}2}, \Gamma_{8'\text{-}2}$	63 $\Gamma_{8\text{-}2}, \Gamma_{8'\text{-}4}$	82 $\Gamma_{6\text{-}2}, \Gamma_{8'\text{-}1}$
7 $\Gamma_{7\text{-}1}, \Gamma_{8\text{-}4}$	26 $\Gamma_{7'\text{-}1}, \Gamma_{7'\text{-}2}$	45 $\Gamma_{7'\text{-}2}, \Gamma_{8'\text{-}3}$	64 $\Gamma_{8\text{-}3}, \Gamma_{8\text{-}4}$	83 $\Gamma_{6\text{-}2}, \Gamma_{8'\text{-}2}$
8 $\Gamma_{7\text{-}1}, \Gamma_{6\text{-}1}$	27 $\Gamma_{7'\text{-}1}, \Gamma_{8\text{-}1}$	46 $\Gamma_{7'\text{-}2}, \Gamma_{8'\text{-}4}$	65 $\Gamma_{8\text{-}3}, \Gamma_{6\text{-}1}$	84 $\Gamma_{6\text{-}2}, \Gamma_{8'\text{-}3}$
9 $\Gamma_{7\text{-}1}, \Gamma_{6\text{-}2}$	28 $\Gamma_{7'\text{-}1}, \Gamma_{8\text{-}2}$	47 $\Gamma_{8\text{-}1}, \Gamma_{8\text{-}2}$	66 $\Gamma_{8\text{-}3}, \Gamma_{6\text{-}2}$	85 $\Gamma_{6\text{-}2}, \Gamma_{8'\text{-}4}$
10 $\Gamma_{7\text{-}1}, \Gamma_{8'\text{-}1}$	29 $\Gamma_{7'\text{-}1}, \Gamma_{8\text{-}3}$	48 $\Gamma_{8\text{-}1}, \Gamma_{8\text{-}3}$	67 $\Gamma_{8\text{-}3}, \Gamma_{8'\text{-}1}$	86 $\Gamma_{8'\text{-}1}, \Gamma_{8'\text{-}2}$
11 $\Gamma_{7\text{-}1}, \Gamma_{8'\text{-}2}$	30 $\Gamma_{7'\text{-}1}, \Gamma_{8\text{-}4}$	49 $\Gamma_{8\text{-}1}, \Gamma_{8\text{-}4}$	68 $\Gamma_{8\text{-}3}, \Gamma_{8'\text{-}2}$	87 $\Gamma_{8'\text{-}1}, \Gamma_{8'\text{-}3}$
12 $\Gamma_{7\text{-}1}, \Gamma_{8'\text{-}3}$	31 $\Gamma_{7'\text{-}1}, \Gamma_{6\text{-}1}$	50 $\Gamma_{8\text{-}1}, \Gamma_{6\text{-}1}$	69 $\Gamma_{8\text{-}3}, \Gamma_{8'\text{-}3}$	88 $\Gamma_{8'\text{-}1}, \Gamma_{8'\text{-}4}$
13 $\Gamma_{7\text{-}1}, \Gamma_{8'\text{-}4}$	32 $\Gamma_{7'\text{-}1}, \Gamma_{6\text{-}2}$	51 $\Gamma_{8\text{-}1}, \Gamma_{6\text{-}2}$	70 $\Gamma_{8\text{-}3}, \Gamma_{8'\text{-}4}$	89 $\Gamma_{8'\text{-}2}, \Gamma_{8'\text{-}3}$
14 $\Gamma_{7\text{-}2}, \Gamma_{7'\text{-}1}$	33 $\Gamma_{7'\text{-}1}, \Gamma_{8'\text{-}1}$	52 $\Gamma_{8\text{-}1}, \Gamma_{8'\text{-}1}$	71 $\Gamma_{8\text{-}4}, \Gamma_{6\text{-}1}$	90 $\Gamma_{8'\text{-}2}, \Gamma_{8'\text{-}4}$
15 $\Gamma_{7\text{-}2}, \Gamma_{7'\text{-}2}$	34 $\Gamma_{7'\text{-}1}, \Gamma_{8'\text{-}2}$	53 $\Gamma_{8\text{-}1}, \Gamma_{8'\text{-}2}$	72 $\Gamma_{8\text{-}4}, \Gamma_{6\text{-}2}$	91 $\Gamma_{8'\text{-}3}, \Gamma_{8'\text{-}4}$
16 $\Gamma_{7\text{-}2}, \Gamma_{8\text{-}1}$	35 $\Gamma_{7'\text{-}1}, \Gamma_{8'\text{-}3}$	54 $\Gamma_{8\text{-}1}, \Gamma_{8'\text{-}3}$	73 $\Gamma_{8\text{-}4}, \Gamma_{8'\text{-}1}$	
17 $\Gamma_{7\text{-}2}, \Gamma_{8\text{-}2}$	36 $\Gamma_{7'\text{-}1}, \Gamma_{8'\text{-}4}$	55 $\Gamma_{8\text{-}1}, \Gamma_{8'\text{-}4}$	74 $\Gamma_{8\text{-}4}, \Gamma_{8'\text{-}2}$	
18 $\Gamma_{7\text{-}2}, \Gamma_{8\text{-}3}$	37 $\Gamma_{7'\text{-}2}, \Gamma_{8\text{-}1}$	56 $\Gamma_{8\text{-}2}, \Gamma_{8\text{-}3}$	75 $\Gamma_{8\text{-}4}, \Gamma_{8'\text{-}3}$	
19 $\Gamma_{7\text{-}2}, \Gamma_{8\text{-}4}$	38 $\Gamma_{7'\text{-}2}, \Gamma_{8\text{-}2}$	57 $\Gamma_{8\text{-}2}, \Gamma_{8\text{-}4}$	76 $\Gamma_{8\text{-}4}, \Gamma_{8'\text{-}4}$	

The Hamiltonian for electrostatic interactions between the f-electrons is given by eq 2

$$H_{ee} = \sum_{k=0,2,4,6} F^k(nf,nf)\, f_k \tag{2}$$

where $F^k(nf,nf)$s represent the radial parts of the electrostatic interaction between f-electrons, which are evaluated empirically.[25] The angular part of these interactions, f_k, can be evaluated exactly. We follow the procedures outlined by Eisenstein and Pryce[36] and utilize the matrix elements of the electrostatic interaction given by Condon and Shortley[41] to evaluate the angular factors, f_ks.

The Hamiltonian for spin-orbit interaction is given by eq 3

$$H_{SO} = \zeta\, l_i \bullet s_i \tag{3}$$

where ζ is the spin-orbit coupling constant, and l_i and s_i are the orbital and spin angular momenta of the electron. In our model, the values of the Slater parameters, F^ks, and the spin-orbit parameter, ζ, are fixed at the values found from fitting the gas phase free ion energy levels. The model was antisymmetrized by antisymmetrizing the matrix elements. For a given matrix element, $\langle f^{(1)}f^{(2)}|O|f'^{(1)}f'^{(2)}\rangle$ is replaced by ½[$\langle f^{(1)}f^{(2)}|O|f'^{(1)}f'^{(2)}\rangle$ - $\langle f^{(2)}f^{(1)}|O|f'^{(1)}f'^{(2)}\rangle$ - $\langle f^{(1)}f^{(2)}|O|f'^{(2)}f'^{(1)}\rangle$ + $\langle f^{(2)}f^{(1)}|O|f'^{(2)}f'^{(1)}\rangle$], where f is an atomic f-orbital.

Free ion spectra for U^{4+}(U V) and Pr^{3+}(Pr IV)

The 13 levels expected for gas phase, free ion U^{4+} (U V) have been reported and assigned.[42] We have used the free ion parameters in Table 2 (calculation 2) of Van Deurzen et al.[42] as the starting point of our work. For the Pr^{3+} (Pr IV) free ion in the gas phase, 12 levels of the expected 13 levels for the $4f^2$ configuration of the Pr IV spectrum have been assigned.[43, 44]

Our model for the electronic structures of $[UX_6]^{2-}$ and $[PrCl_6]^{3-}$ does not include the configuration interaction parameters α, β, and γ or the effective operators, M^k and P^k. Instead we compensated for this omission by the following procedure. We used all the U^{4+} and the Pr^{3+} free ion parameters (as given in Table 3), including the configuration interaction parameters and the effective operators plus the crystal field parameters from earlier studies[11, 22, 45] (given in Table 4) and calculated the energy levels in the S L J m_J representation. Then we did a second calculation with the same free ion values for the $F^k s$ and ζ and the crystal field parameters (again in S L J m_J representation) but did not include α, β, γ, M^k, or P^k. Subtracting the eigenvalues from the calculation with configuration interaction and the effective operators from the second calculation gave correction energies for each calculated crystal field level. These correction energies were applied to each of the calculations and fitting programs in the octahedral, $m_s^{(1)}$, $m_l^{(1)}$, $m_s^{(2)}$, $m_l^{(2)}$ basis set as appropriate for the complex under study.

Table 3. Free ion parameter values in cm^{-1} for U^{4+} and Pr^{3+}

Parameter	U^{4+} free ion	Pr^{3+} free ion
F^2	51909	71822
F^4	42721	51827
F^6	27710	33890
ζ	1969	766
α	35.6	23.9
β	-669	-599
Γ	763	1400
M^0	0.987	1.98
M^2	0.550	0.56 M^0
M^4	0.384	0.38 M^0
P^2	495	166
P^4	0.75 P^2	0.75 P^2
P^6	0.50 P^2	0.50 P^2
Reference	42	44

Table 4. Empirical crystal field parameters in cm^{-1} for U^{4+} and Pr^{3+} complexes with octahedral crystal fields

Parameter	$[UF_6]^{2-}$	$[UCl_6]^{2-}$	$[UBr_6]^{2-}$	$[UBr_6]^{2-}$	$[UBr_6]^{2-}$	$[UI_6]^{2-}$	$[PrCl_6]^{3-}$
F^2	49699	41288	41198	40290	42313	38188	67647
F^4	0.74 F^2	39966	35393	35878	36881	0.74 F^2	48950
F^6	0.55 F^2	26502	25766	23657	23202	0.55 F^2	31963
ζ(r)	1970	1801	1804	1772	1817	1724	752.5
α		9.7	17.6	21.38	34.7		23.5
β				-455	-883		-690
γ				1573	2108		1684
B_0^4	10067	7525	6956	6823	12385	6338	1996
B_0^6	22	1432	1149	1310	2468	941	222
# of levels fit	16	22	34	34	34	11	38
# of variables	4	7	7	9	14 [b]	4	10
σ (cm^{-1}) [a]	60	182	287	246	54	165	38
Reference	29	22	22	11	11	29	13

[a] $\sigma = \Sigma[(\Delta i)^2/(n - p)]^{1/2}$ where Δi is the difference between the observed and calculated levels, n is the number of excited states fit, and p is the number of parameters varied. The values for previous studies were calculated from the reported calculated and experimental values.

[b] There were 8 additional parameters for this fit, some values were fixed. See reference [11] for details.

MO model for two equivalent f-electrons in an octahedral complex ion, MX_6^{2-}

As discussed above, an octahedral crystal field splits the f-orbitals into orbitals with t_{1u}, t_{2u}, and a_{2u} symmetry. Overlap between the f-orbitals and ligand orbitals allows the orbitals to mix to produce the corresponding MOs. Following the approach used by Thornley, these MOs are given in Scheme 1, where the atomic f-orbitals are represented by f_i and the corresponding MOs are represented by φ_i.[8] The f-orbital character of these antibonding MOs is given by the normalization factors N_{t1u}, N_{t2u}, and N_{a2u}, which reflect the orbital mixing of the interaction between the metal and ligand orbitals.

$$\varphi_x = N_{t1u}\left[f_x - \tfrac{1}{2}\lambda_\pi\left(-x_3 - x_6 - x_2 - x_5\right) - \sqrt{\tfrac{1}{2}}\lambda_\sigma\left(-\sigma_1 - \sigma_4\right)\right]$$

t_{1u} $$\varphi_y = N_{t1u}\left[f_y - \tfrac{1}{2}\lambda_\pi\left(-y_1 - y_4 - y_3 - y_6\right) - \sqrt{\tfrac{1}{2}}\lambda_\sigma\left(-\sigma_2 - \sigma_5\right)\right]$$

$$\varphi_z = N_{t1u}\left[f_z - \tfrac{1}{2}\lambda_\pi\left(-z_2 - z_5 - z_1 - z_4\right) - \sqrt{\tfrac{1}{2}}\lambda_\sigma\left(-\sigma_3 - \sigma_6\right)\right]$$

$$\varphi_\xi = N_{t2u}\left[f_\xi - \tfrac{1}{2}\lambda'_\pi\left(-x_3 - x_6 + x_2 + x_5\right)\right]$$

t_{2u} $$\varphi_\eta = N_{t2u}\left[f_\eta - \tfrac{1}{2}\lambda'_\pi\left(-y_1 - y_4 + y_3 + y_6\right)\right]$$

$$\varphi_\zeta = N_{t2u}\left[f_\zeta - \tfrac{1}{2}\lambda'_\pi\left(-z_2 - z_5 + z_1 + z_4\right)\right]$$

a_{2u} $$\varphi_{a2u} = N_{a2u} f_{a_2}$$

$$N_{t2u}^2 = \left(1 + \lambda'^2_\pi\right)^{-1} \qquad N_{t1u}^2 = \left(1 + \lambda_\pi^2 + \lambda_\sigma^2\right)^{-1} \qquad N_{a2u}^2 = 1$$

Scheme 1. Thornley's MO model applied to an octahedral f^l complex using an sp-hybridized σ–bonding orbital rather than separate s and p-orbitals. The ligand σ-orbitals are represented as "σ", while the ligand π_x, π_y, and π_z-orbitals are represented by "x," "y," and "z," respectively. The contribution from the overlap regions has been removed from the formulas for the normalization constants.

These wave functions form an octahedral basis set, so the crystal field interaction is diagonal. The crystal field interaction for the two f-electrons is just the sum of the interaction for electron one and electron two. Since the a_{2u} orbital is lowest in energy, we set this state equal to 0 cm^{-1} (e_3 = 0). The energy of the t_{1u} orbital is ε_1, and the energy of the t_{2u} orbital is ε_2 (Figure 1). For simplicity, we perform our calculations using two scaling factors based on the the initial values of ε_1 and ε_2, from which B_0^4 and B_0^6 in Tables 7 and 8 are determined. Otherwise, the crystal field splitting of the orbitals is handled identically to a conventional crystal field model in that orbital mixing is not explicity included; the crystal field parameters, and the final values for ε_1 and ε_2, are the empirically derived energies of the t_{1u} and t_{2u} orbitals relative to the a_{2u} orbital.

As noted above, the matrix elements for spin-orbit coupling and electrostatic interaction are calculated from values of ζ and F^ks found for the gas phase free ions, which are not varied. Instead, the effect of orbital mixing on these interactions are modeled using the approach used by Lohr for transition metal systems and outlined by Judd for actinides.[38, 40] Briefly, the matrix elements for the interactions in the complex ion are modeled by multiplying the matrix elements for the free ion by the normalization factors for the electrons involved in the initial and final states. This approach led us to use the $m_s^{(1)}$, $m_l^{(1)}$,$m_s^{(2)}$, $m_l^{(2)}$ basis rather than the usual L S J m_J basis. Modeling the effects of orbital mixing on the matrix elements is more straightforward in the former basis.

The spin-orbit operator depends only on the coordinates of one electron and thus can be separated into a sum of matrix elements for electron 1 and elctron 2.[41] To model the effect of

orbital mixing on the spin-orbit interaction, we first calculate the matrix element for the atomic f-orbitals, $\langle f|H_{SO}|f'\rangle$. The spin-orbit interaction matrix element in the complex, $\langle \varphi|H_{SO}|\varphi'\rangle$ is given by eq 4 or 5 for calculation without and with the orbital reduction factor, respectively, where N_φ is the normalization constant for the molecular orbital occupied by the f-electron and $k_{\varphi\varphi'}$ is the corresponding orbital reduction factor given in Table 5.[8, 9] As discussed below, we evaluated spin-orbit coupling both with and without orbital reduction.

$$\langle \varphi|H_{SO}|\varphi'\rangle = N_\varphi N_{\varphi'}\langle f|H_{SO}|f'\rangle \tag{4}$$

$$\langle \varphi|H_{SO}|\varphi'\rangle = N_\varphi N_{\varphi'} k_{\varphi\,\varphi'}\langle f|H_{SO}|f'\rangle \tag{5}$$

Table 5: Definitions for determining orbital reduction factors from the values of N_{t2u} and N_{t1u}

Orbital reduction factors	
$\alpha_\pi^2 = \frac{3}{5}\left(\frac{1}{N_{t_{2u}}^2} - 1\right)$	$k_{t_{1u}t_{1u}} = 1 - N_{t_{1u}}^2\left[\frac{4}{3}\alpha_\pi^2 + \alpha_\sigma^2 + \frac{2\sqrt{2}}{3}\alpha_\pi\alpha_\sigma\right]$
$\alpha_\sigma^2 = \frac{1}{N_{t_{1u}}^2} - \frac{3}{5N_{t_{2u}}^2} - \frac{2}{5}$	$k_{t_{2u}t_{2u}} = 1 - 2N_{t_{2u}}^2\alpha_\pi'^2$
$\alpha_\pi'^2 = \frac{1}{N_{t_{2u}}^2} - 1$	$k_{a_{2u}t_{2u}} = 1 - \frac{1}{2}N_{t_{2u}}\alpha_\pi'^2$
	$k_{t_{1u}t_{2u}} = 1 - N_{t_{1u}}N_{t_{2u}}\left[\frac{1}{2}\left(\alpha_\pi^2 + \alpha_\pi'^2 + \alpha_\sigma^2\right) + \sqrt{\frac{2}{15}}\alpha_\pi'\left(\alpha_\sigma - \frac{2\alpha_\pi}{\sqrt{2}}\right)\right]$

The effect of orbital mixing on electron repulsion is treated similarly except that the this operator depends on the coordinates of both electrons as shown in eq 6

$$\langle \varphi^{(1)},\varphi^{(2)}|H_{ee}|\varphi'^{(1)},\varphi'^{(2)}\rangle = N_{\varphi(1)}N_{\varphi(2)}N_{\varphi'(1)}N_{\varphi'(2)}\langle f^{(1)},f^{(2)}|H_{ee}|f'^{(1)},f'^{(2)}\rangle \quad (6)$$

where $^{(1)}$ and $^{(2)}$ denote electron 1 and electron 2, respectively, of the two-electron wave function. H_{ee} is calculated as described above, and $\langle \varphi^{(1)},\varphi^{(2)}|$ and $|\varphi'^{(1)},\varphi'^{(2)}\rangle$ are the two of the 91 two-electron wave functions shown in Table 2.

Under a crystal field of O_h symmetry, the 91 levels expected for two equivalent f-electrons are split into five groups consisting of seven Γ_1 singlets, three Γ_2 singlets, nine Γ_3 doublets nine Γ_4 triplets, and twelve Γ_5 triplets for a total of 91 levels.[46] Our programs calculate matrix elements for all 91 states and do not make use of group theory. Consequently, after each diagonalization of the 91 by 91 matrix, a subroutine sorts the 91 eigenvalues into three groups (ten singlets, nine doublets, and twenty-one triplets), and assigns a unique number to each of the levels of each group. This unique number is used to relate the calculated level to an assigned level in the experimental spectra, which use a similar classification system.

Fortran routines were written for calculating the necessary matrix elements utilizing the wave functions given in Tables 2 and 3. This program varied the orbital mixing parameters N_{t1u} and N_{t2u} ($N_{a2u} = 1$ since the a_{2u} f-orbital is nonbonding) and the two crystal field parameters ε_1 and ε_2 to minimize the differences between the calculated energy levels and the experimentally assigned energy levels. The starting values in our fitting scheme are the free ion parameters given in Table

4 for the Pr^{3+} and U^{4+} ions and the crystal field parameters given for each anionic complex. We then varied the parameters N_{t1u} and N_{t2u} keeping ε_1 and ε_2 set at the values given in Table 1. After the first iteration, the values of N_{t1u} and N_{t2u} were fixed at the values found after the first iteration, and ε_1 and $\varepsilon_2$were allowed to vary. For the last iteration, all four parameters, N_{t1u}, N_{t2u}, ε_1, and ε_2 were allowed to vary. The starting values of the parameters were then varied until no further improvement in the fit was obtained. Lists of experimental and calculated energy levels are provide in the supplementary information (SI).

Results

The results of our calculations for five sets of data, $[UX_6]^{2-}$ (X=F, Cl, Br, I) and $[PrCl_6]^{3-}$, without and with the inclusion of the orbital redution factors in the evaluation of the spin-orbit interacton, are given in Tables 6 and 7, respectively. Our simple model, involving only four variable parameters, provides results which are comparable to those obtained with more extended crystal field models using at least 7 variable parameters (Table 4). The more extensive model of Faucher et al., which includes the mixing of 7p states, provides much better agreement with the experimental data as shown in Table 4. However, this model employed 17 parameters of which 14 were allowed to vary.

Table 6. Results from fitting of parameters N_{t1u}, N_{t2u}, ε_1, and ε_2 without orbital reduction.

	$[UF_6]^{2-}$	$[UCl_6]^{2-}$	$[UBr_6]^{2-}$	$[UI_6]^{2-}$	$[PrCl_6]^{3-}$
N_{t1u}	0.963	0.942	0.939	0.821	0.987
N_{t2u}	1.004	0.940	0.934	0.908	0.981
ε_1 (cm^{-1})	5386	3462	2972	2775	1036
ε_2 (cm^{-1})	3469	1000	435	803	200
B_0^4 (cm^{-1})	9516	7040	6361	5641	2181
B_0^6 (cm^{-1})	-598	1158	1524	926	470
n	16	21	34	11	37
σ (cm^{-1})[a]	128	142	242	115	86

[a] $\sigma = \Sigma[(\Delta i)^2/(n - p)]^{1/2}$ where Δi is the difference between the observed and calculated energies, n is the number of excited states, and p = 4, the number of parameters varied.

Table 7. Results from fitting of parameters N_{t1u}, N_{t2u}, ε_1, and ε_2 including orbital reduction.

	$[UF_6]^{2-}$	$[UCl_6]^{2-}$	$[UBr_6]^{2-}$	$[UI_6]^{2-}$	$[PrCl_6]^{3-}$
N_{t1u}	0.976	0.935	0.936	0.891	0.985
N_{t2u}	1.003	0.965	0.962	0.949	0.984
ε_1 (cm^{-1})	5491	3441	2902	2876	1032
ε_2 (cm^{-1})	3404	1104	533	438	188
B_0^4 (cm^{-1})	9802	6914	6129	6142	2180
B_0^6 (cm^{-1})	-443	1012	1352	1454	483
n	16	21	34	11	37
σ (cm^{-1})[a]	120	227	296	160	112

[a] $\sigma = \Sigma[(\Delta i)^2/(n - p)]^{1/2}$ where Δi is the difference between the observed and calculated levels, n is the number of excited state energies fit, and p = 4, the number of parameters varied.

Correcting for configuration interaction was essential for obtaining acceptable agreement between the experiemental results and the calculated energies. Our ad hoc inclusion of configuration interaction in our model, descibed above, resulted in a marked improvement in the fitting results. As noted above, the agreement between our model and data are not as good as in some previous studies. A number of factors contribute to the poorer agreement with experiment in our model. First is the ad hoc treatment of the cofiguration interaction and magnetic parameters. The assumption that orbital mixing has no effect on these parameters is certainly not true. Second is the implicit assumption that the decrease in the values of the Slater parameters and spin-orbit coupling constant is due solely to the decreased f-orbital character of the antibonding MOs created by orbital mixing. While this is the major contributor, these parameters

are also decreased due to overlap between the occupied ligand orbitals and the unoccupied metal s, p, and d orbitals (central field covalence). These interactions result in slight screening of the f orbitals, which also reduces the electron repusion and spin-orbit paramaters. In transition metals, this decrease ranges from 1% in $KNiF_3$ to 15% in $FeCl_4^-$ complexes.[47, 48] In our previous study of f^1 systems, this decrease was approximately 5% in NpF_6.[9] Since central field covalence is not included in our model, our orbital mixing parameters, N_{t1u} and N_{t2u}, will be slightly smaller than they would be if central field covalence were included.

The crystal field parameters may be compared with previous work (direct comparisons are given in the SI). In comparison to previous crystal field fits, the values of B_0^4 and B_0^6 are similar although systematically smaller. The notable exception is the model of the electronic structure of UBr_6^{2-} by Faucher and coworkers, for which the values of B_0^4 and B_0^6 are much larger.[11] Splitting of the f-orbitals has been calculated using wavefuncation methods (CASSCF) by Jung, et al.[35] Using these values of e_σ and e_π, the t_{1u} and t_{2u} orbitals are 3511 cm^{-1} and 1208 cm^{-1} higher in energy than the a_{2u} in UCl_6^{2-}, which are in good agreement with ε_1 and ε_2 in Tables 6 and 7. For $PrCl_6^{3-}$, the corresponding values are 702 cm^{-1} and 233 cm^{-1}. In this case, calculated energy of the t_{1u} orbital is much smaller than the value determinued using our model, ca. 1040 cm^{-1}. The discrepency between the observed and calculated 4f-orbital splitting in octahedral lanthanide hexahalide complexes has previously observed and discussed for CASSCF.[49] The splitting of the 4f obitals in $PrCl_6^{3-}$ is in good agreement with that calculated by DFT.[50]

The degree of orbital mixing determined using our model may be compared to the other studies. As expected, very little orbital mixing is observed in $PrCl_6^{3-}$, and the degree of mixing is in agreement with earlier computational studies.[49, 50] Likewise, the calculated orbital mixing coefficents of the t_{1u} and t_{2u} orbitals in UCl_6^{2-} are 0.94 and 0.97, which are slightly larger than the values of N_{t1u} and N_{t2u}.[35] Minasian, et al. studied UCl_6^{2-} by Cl K-edge XANES spectroscopy, which provides the degree of Cl 3p orbital mixing.[32] For each chloride ligand, the total amount of Cl 3p character in both the t_{1u} and t_{2u} orbitals was found to be 5.7 %, which corresponds to 34 % for the entire complex. In our model, the amount of Cl 3p character in the f-orbitals is given by $[3(1-N_{t1u}^2)+3(1-N_{t2u}^2)]$, where the factor of 3 accounts for the spatial degeneracies of the orbitals. For comparison with the values determined by Cl K-edge XANES spectroscopy, this value must be normalized by ½, which is the fraction of ungerade Cl 3p orbitals that mix with the 5f orbitals relative to the total number of Cl 3p orbitals in UCl_6^{2-}. For UCl_6^{2-}, we find that the Cl charcter in 5f orbitals is 28 % or 35 % for the models with and without orbital reduction, respectively, which are in good ageement with the value of 34% determined by Minasian, et al.

The model used here may be checked for internal consistency by comparing the values of N_{t1u} and N_{t2u} with the orbital mixing determined from ε_1 and ε_2 using second order perturbation theory.[51, 52] As shown by Burdett, the interaction energy, Δe_i, which is the change in energy of orbital φ_i due to interaction with orbital φ_j, is given by eq 7

$$\Delta e_i = \frac{\left(H_{ij} - S_{ij}e_i\right)^2}{\left(e_i - e_j\right)} \tag{7}$$

where e_i and e_j are the unperturbed energies, H_{ij} is the interaction integral (hopping integral), and S_{ij} is the overlap integral. H_{ij} may be approximated by the Wolfsberg-Helmholz approximation, $H_{ij} \approx S_{ij}(e_i + e_j)$.[51, 52] Using this approximation, the interaction energy is given by eq 8 as shown by Burdett.[52] The value of the mixing parameter, λ, may be determined in the same way (eq 9). The normalization parameter is given by eq 10. The energies of the unperturbed ligand orbitals, e_X, may be estimated using the ionization energies of the halogen atoms as previously done.[9] The energy of the unperturbed f-orbitals, e_M, in U(IV) may be roughly estimated by using the fourth ionization potential, 35.75 eV, divided by 4, which is 8.9 eV. This value may be compared to the ionization energies of UBr_4, UCl_4, and UF_4, which are 9.6 eV, 9.2 eV, and 9.5 eV, respectively.[53, 54] The energy of the Pr(III) f-orbitals was simlarly estimated from the third ionization potential of Pr, 22.1 eV, divided by 3, which is 7.4 eV.[55] This value is in good agreement with the 4f ionization energy of $(C_5H_5)_3Pr$, 7.33 eV, but not in good agreement with the ionization energy of $PrCl_3$ in the gas phase, 11.4 eV.[55-57] The ionization potentials, estimated overlap integrals, and the values of N determined from ε_1 and ε_2 are given in Table 8 using the values from Table 7. The values for the model without orbital reduction (Table 6) are almost identical.

$$\Delta e_i \approx \frac{\left(S_{ij} e_j\right)^2}{\left(e_i - e_j\right)} \tag{8}$$

$$\lambda = \frac{\left(S_{ij} e_j\right)}{\left(e_i - e_j\right)} \tag{9}$$

$$N = \sqrt{\frac{1}{1+\lambda^2}} \tag{10}$$

Table 8. Estimated orbital energies of the metal (e_M) and ligand (e_X), overlap integrals and metal orbital character determined from ε_1 and ε_2 in Table 7 (model with orbital reduction)

	UF_6^{2-}	UCl_6^{2-}	UBr_6^{2-}	UI_6^{2-}	$PrCl_6^{2-}$
e_M (eV)	-8.9	-8.9	-8.9	-8.9	-7.4
e_X (eV)	-17.4	-13.0	-11.8	-10.5	-13.0
S_{t1u}	0.14	0.10	0.09	0.07	0.07
S_{t2u}	0.11	0.06	0.04	0.03	0.03
N_{t1u} (est)	0.96	0.95	0.94	0.90	0.99
N_{t2u} (est)	0.98	0.98	0.99	0.98	1.00

Comparison on the values of N_{t1u} and N_{t2u} in Table 8 with those in Tables 6 and 7 shows that the values are in good agreement, especially for the model that includes orbital reduction. The estimated overlap integrals may be compared to those calculated for UCl_6^{2-} calculated using DFT by Su et al., who find 0.29 and 0.21 for the t_{1u} and t_{2u} orbitals, respectively.[33] These values are in greement with $3S_{t1u}$ and $3S_{t1u}$ for UCl_6^{2-}, 0.31 and 0.19 (the factor of 3 accounts for the spatial degeneracy of the t_{1u} and t_{2u} orbitals). These results indicate that the model is internally consistent in that the degree of orbital mixing and metal character in the t_{1u} and t_{2u} orbitals that can be estimated from the destabilization of these orbitals is in good agreement with the metal character determined by the model. Internal consistentancy does not prove that the model is accurate; however, a lack of internal consistency would have indicated a problem with the model.

Discussion

Our main goal in using this model is to expore how the interactions between the the metal and ligand orbitals affect orbital mixing (N_{t1u} and N_{t1u}) and destabilization of the antibonding orbitals (ε_1 and ε_2). However, the behavior of these orbitals is not particularly relevant to the relative stabilities of the compounds. Stabilization of the corresponding bonding orbitals is more relevant in this respect, and these values may be estimated using eq 11, which is determined by taking the ratio of eq 8 for the antibonding and bonding orbitals. The estimated stabilization of the ligand orbitals due to f-orbital interactions are given in Table 9 along with the total crystal field stabilzation of the ligands, $6(\Delta e_{X\text{-}t1u}+\Delta e_{X\text{-}t2u})$. Given the assumptions used here, especially the assumptions about the energies of the unperturbed ligand and metal orbitals, the estimated stabilization of the ligand orbitals may not be accurate. However, the trends in the energies are still valid. The trend in stabilization of the ligand orbitals is surprising in that there is little variation across the series, which is certainly in conflict with our expectation that the fluoride complex would be much more stable than the iodide complex. It should be noted that the stabilization shown in Table 9 is due only to interaction with the metal f-orbitals. The d-orbitals have much greater overlap with the ligand orbitals and are more important in stabilizing the complexes. In addition, these complexes are stabilized by electrostatic effects, which are largest in UF_6^{2-} since it has the shortest U-X distance.

$$\Delta e_i \approx \left(\frac{e_j}{e_i}\right)^2 \Delta e_j \qquad (11)$$

Table 9. Stabilization of the t_{1u} and t_{2u} ligand orbitals (model with orbital reduction)

	UF_6^{2-}	UCl_6^{2-}	UBr_6^{2-}	UI_6^{2-}	$PrCl_6^{2-}$
$\Delta e_{X\text{-}t1uu}$ (cm^{-1})	-1437	-1613	-1651	-2068	-331
$\Delta e_{X\text{-}t2uu}$ (cm^{-1})	-891	-517	-303	-315	-60
Total (cm^{-1})	-13963	-12781	-11724	-14299	-2346

The trends in orbital energies across the series of uranium complexes are illustrated in Figure 2, which shows considerable variation among the bonding and antibonding oribtals. The destabilization of the antibonding orbitals (ε_1 and ε_2) decreases strongly from X = F to I. The stabilization of the ligand π orbitals due to interaction with the f-orbitals ($\Delta e_{X\text{-}t2u}$) decreases slightly along the series, and the stabilization of the σ and π bonding ligand orbitals ($\Delta e_{X\text{-}t1u}$) increases slightly across the series. These trends illustrate the impacts of absolute orbital energy and overlap, which are in the numerator in eq 8 and 9 and relative orbital energy, which is in the denominator. All of the trends may be understood using eq 8.[52]

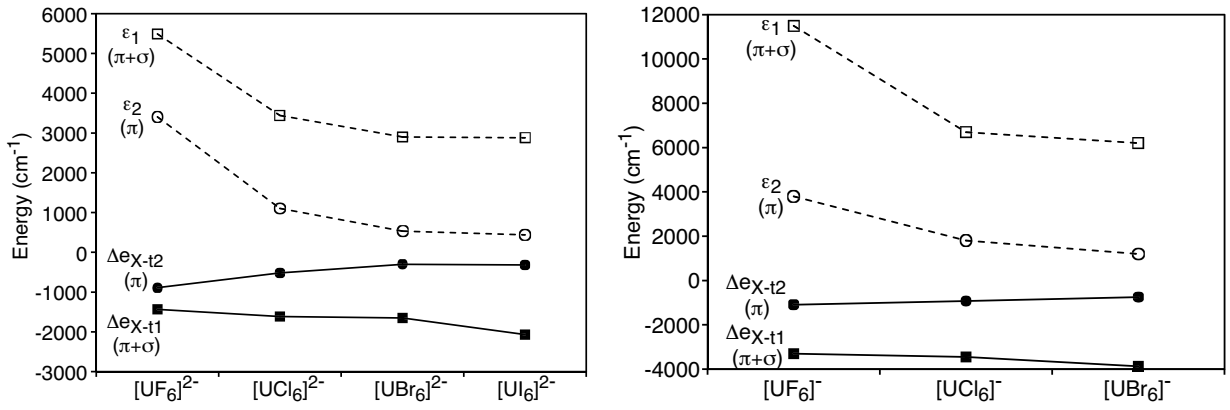

Figure 2. Changes in orbital energy among U(IV) hexahalide complexes(left) and U(V) hexahalide complexes (right). Empty symbols are the destabilzation of the f-orbitals, and filled symbols are the stabilization of the ligand orbitals.

The trend in destabilization of the antibonding f-orbitals is dominated by overlap and the stability of the ligand orbitals both of which decrease drastically from fluoride through iodide. The trends in the stabilization of the ligand orbitals are more interesting since the energy of U(IV) does not change across the series, so changes in orbital energies are due only to changes in overlap and the relative energies of the ligand and metal orbitals. The behavior of the ligand π orbitals is dominated by a drop in overlap from UF_6^{2-} to UI_6^{2-}, which has a greater influence than the relative orbital energies. On the other hand, the ligand t_{1u} orbital trend is dominated by relative energies of the metal and ligand orbitals because overlap decreases less strongly across the series. It should be noted, however, that minimizing the relative energy of the ligand and metal orbitals alone does not produce significant stabilization of the ligand orbitals. Stabilization requires some degree of overlap between the orbitals. In the case of the t_{1u} orbitals, the overlap

changes little across the series, so the trend in orbital energies is dictated by the relative orbital energies.

The role of changing the oxidation state of the metal may be examined using the bonding parameters for U(V) hexahalide complexes, which are summarized in Table 10.[9] The properties and state energies of UF_6^-, UCl_6^-, and UBr_6^- have also been modeled using wave function calculations.[58-62] The corresponding trends in the energies of the orbitals are shown in Figure 2. Within the U(V) complexes, the trends are the same as for the U(IV) hexahalide complexes. More interesting is the trend going from U(IV) complexes to U(V) complexes. The estimated energy of the U(V) orbitals is -9.33 eV,[9] so for U(V), the 5f orbitals are closer in energy to the ligand orbitals than for U(IV). In addition, the ionic radius of U(V) is smaller than that of U(IV), which leads to shorter U-X bonds and greater overlap. These differences result in greater orbital mixing among U(V) complexes, stronger destabilation of the f-orbitals, and greater stabilization of the ligand orbitals.

Table 10. Bonding parameters for U(V) hexahalide complexes[9]

	UF_6^-	UCl_6^-	UBr_6^-
ε_1	11500	6700	6200
ε_2	3800	1800	1200
N_{t1u}	0.93	0.90	0.87
N_{t2u}	0.98	0.98	0.97
S_{t1u}	0.19	0.13	0.12
S_{t2u}	0.11	0.07	0.05
$\Delta e_{X\text{-}t1uu}$ (cm^{-1})	-3306	-3451	-3876
$\Delta e_{X\text{-}t2uu}$ (cm^{-1})	-1093	-927	-750
N_{t1u} (est)	0.92	0.90	0.87
N_{t2u} (est)	0.97	0.97	0.97

Conclusions

We have developed a new version of the crystal field model for describing the the electronic structure of octahedral f^2 complexes in terms of f-orbital splitting and mixing of the metal f-orbitals and ligand orbitals. The treatment of f-orbital splitting is the same as previously done with crystal field models, but the treatment of orbital mixing is new. Using a framework originally described by Judd, we have modeled the decreases in the Slater parameter and spin-orbit coupling by multiplying the free-ion matrix elements by the f-orbital character of the MOs involved in the interaction. In addition, it was necessary to correct for higher order configuration and magnetic interactions, which was done in an ad hoc manner using the results from existing crystal field calculations. The new model uses only 4 parameters to describe the electronic structure, and unsurprisingly does not necessarily model the data as well as existing models that use more parameters. Nevertheless, it still models the data well. The model that does not include orbital reduction has better agreement with the experimental values than the model that does include orbital reduction.

Our model has the following advantages. We can use as starting parameters the empirically determined free ion parameters for the U^{4+} and Pr^{3+} ions. Secondly, only four parameters are needed for the application of this model. Two orbital mixing parameters arise directly from MO theory and are used to account for the changes to the electrostatic and spin-orbit matrix elements, and the other two parameters are determined by the scaling of the two empirical crystal field parameters to account for the destabilization of the f-orbitals due to antibonding interactions with the ligands. Finally, our model allows the degree of orbital mixing in each metal orbital to be determined independently.[4]

The primary advantage of the new model is that it allows one to determine the amount of metal character in the antibonding orbitals in addition to the energies of these orbitals. The metal character may be used to show that the model is internally consistent, which requires that the energies of the metal and ligand orbitals can be estimated. Using these estimated energies, the overlap integrals and energies of the ligand orbitals can also be estimated using second order perturbation molecular orbital theory. These combined parameters allow one to examine the factors that affect bonding in this series of complexes. The three main factors are absolute orbital energies, overlap, and difference in energy between the ligand and metal orbitals. The latter two are well known, but the first has largely been overlooked despite work by Burdett that demonstrated the same principle in transition metal complexes.

Supporting Information Available

The Supporting Information is available free of charge at

Tables S1-S10 of experimental and calculated energies for the crystal field fits, and Tables S11-S15 comparing the crystal field parameters derived here with those previously derived using other models.

Acknowledgements

We wish to thank Dr. Corwin Booth for providing computer resources and for his assistance with the analysis programs. This work was supported by U.S. Department of Energy, Basic Energy Sciences, Chemical Sciences, Biosciences, and Geosciences Division, Heavy Element Chemistry

Program and was performed at Lawrence Berkeley National Laboratory under Contract No. DE-AC02-05CH11231.

References

1. Bethe, H., Termaufspaltung in Kristallen. *Annalen der Physik* **1929,** *395*, 133-208.
2. Van Vleck, J. H., Theory of the Variations in Paramagnetic Anisotropy Among Different Salts of the Iron Group. *Phys. Rev.* **1932,** *41*, 208-215.
3. Jorgensen, C. K.; Pappalardo, R.; Schmidtke, H. H., Do the "Ligand Field" Parameters in Lanthanides Represent Weak Covalent Bonding? *J. Chem. Phys.* **1963,** *39*, 1422-1430.
4. Axe, J. D.; Burns, G., Influence of Covalency upon Rare-Earth Ligand Field Splittings. *Phys. Rev.* **1966,** *152*, 331-340.
5. Alessandri, R.; Zulfikri, H.; Autschbach, J.; Bolvin, H., Crystal Field in Rare-Earth Complexes: From Electrostatics to Bonding. *Chemistry – A European Journal* **2018,** *24*, 5538-5550.
6. Stevens, K. W. H.; Pryce Maurice Henry, L., On the Magnetic Properties of Covalent XY_6 Complexes. *Proc R. Soc. Series A, Math. and Phys. Sci.* **1953,** *219*, 542-555.
7. Judd, B. R., Ligand-Field Theory for Actinides. *J. Chem. Phys.* **1977,** *66*, 3163-3170.
8. Thornley, J. H. M., Covalency in Octahedrally Coordinated Yb^{3+}. *Proc. Phys. Soc.* **1966,** *88*, 325.
9. Lukens, W. W.; Edelstein, N. M.; Magnani, N.; Hayton, T. W.; Fortier, S.; Seaman, L. A., Quantifying the sigma and pi Interactions between U(V) f Orbitals and Halide, Alkyl, Alkoxide, Amide and Ketimide Ligands. *J. Am. Chem. Soc* **2013,** *135*, 10742-10754.
10. Eisenstein, J. C.; Pryce, M. H. L., Theory of the Magnetic and Spectroscopic Properties of Neptunium Hexafluoride. *Proc. R. Soc. London, A* **1960,** *A255*, 181-98.
11. Faucher, M. D.; Moune, O. K.; Garcia, D.; Tanner, P., Evidence for Strong Interaction Between the $5f^2$ and $5f^17p^1$ Configurations of U^{4+} in the Octahedral Sites of Cs_2UBr_6 and Cs_2ZrBr_6. *Phys Rev B* **1996,** *53*, 9501-9504.
12. Faucher, M. D.; Tanner, P. A., Configuration Interaction of Er^{3+} with a Charge Transfer Configuration in the Elpasolite Compound $Cs_2NaErCl_6$. *Mol. Phys.* **2003,** *101*, 983-992.
13. Tanner, P. A., Mak, C. S. K., Faucher, M. D., Configuration Interaction of Pr^{3+} in $PrCl_6^{3-}$. *J. Chem. Phys.* **2001,** *114*, 10860.
14. Johnston, D. A.; Satten, R. A.; Schreiber, C. L.; Wong, E. Y., Covalency Effects in U^{4+} Halide Complexes. *J. Chem. Phys.* **1966,** *44*, 3141.
15. Satten, R. A.; Johnston, D. R.; Wong, E. Y., Zeeman Splitting of Vibronic Levels for Octahedral Actinide and Lanthanide Complexes, Free and in Crystals. *Phys. Rev.* **1968,** *171*, 370.
16. Satten, R. A.; Schreiber, C. L.; Wong, E. Y., Energy Levels of U^{4+} in an Octahedral Crystalline Field. *J. Chem. Phys.* **1965,** *42*, 162.
17. Satten, R. A.; Schreiber, C. L.; Wong, E. Y., Vibronic Intensity Parametrization for the UCl_6^{2-} Complex in Crystals. *J. Chem. Phys.* **1983,** *78*, 79-87.
18. Satten, R. A.; Young, D.; Gruen, D. M., Preliminary Analysis of U^{4+} Ion Spectra in Crystals. *J. Chem. Phys.* **1960,** *33*, 1140.

19. Flint, C. D.; Tanner, P. A., Vibronic Spectra of U^{4+} in Octahedral Crystal Fields I. 647.1 nm Excited Luminescence Spectrum of Cs_2ZrBr_6: UBr_6^{2-}. *Mol. Phys.* **1984,** *53*, 429.
20. Flint, C. D.; Tanner, P. A., Vibronic Spectra of U^{4+} in Octahedral Crystal Fields II. 488 nm Excited Luminescence Spectrum of Cs_2ZrBr_6:UBr_6^{2-}. *Mol. Phys.* **1984,** *53*, 437.
21. Flint, C. D.; Tanner, P. A., Vibronic Spectra of U^{4+} in Octahedral Crystal Fields III. 514.5 nm Excited Infrared Luminescence Spectrum of Cs_2TeBr_6:UBr_6^{2-}. *Mol. Phys.* **1984,** *53*, 801.
22. Flint, C. D.; Tanner, P. A., Vibronic Spectra of U^{4+} in Octahedral Crystal Fields IV. Absorption Spectra and Crystal Field Calculations. *Mol. Phys.* **1987,** *61*, 389.
23. Crosswhite, H. M.; Crosswhite, H., Parametric Model for f-Shell Configurations. I. The Effective-operator Hamiltonian. *J. Opt. Soc. Am. B* **1984,** *1*, 246.
24. Judd, B. R.; Crosswhite, H. M.; Crosswhi.H, Intra-Atomic Magnetic Interactions for f Electrons. *Phys. Rev.* **1968,** *169*, 130-+.
25. Carnall, W. T., A Systematic Analysis of the Spectra of Trivalent Actinide Chlorides in D_{3h} Site Symmetry. *J. Chem. Phys.* **1992,** *96*, 8713-8726.
26. Du Preez, J. G. H.; Rossouw, W. J.; Wiechers, G., Chemistry of Uranium. IV. Electronic Spectral Analysis of Some Six Coordinated Uranium(IV) Complexes. Theoretical Aspects. *S. Afr. J. Chem.* **1972,** *25*, 349-361.
27. Faucher, M. D.; Tanner, P. A.; Mak, C. S. K., Electronic Spectra and Configuration Interaction of Tm^{3+} in $TmCl_6^{3-}$. *J. Phys. Chem. A* **2004,** *108*, 5278-5287.
28. Hubbard, J.; Rimmer, D. E.; Hopgood, F. R. A., Weak Covalency in Transition Metal Salts. *Proc. Phys. Soc.* **1966,** *88*, 13-36.
29. Wagner, W.; Edelstein, N.; Whittaker, B.; Brown, D., Spectral Properties of $(Et_4N)_2UI_6$ and $(Et_4N)_2UF_6$. *Inorg. Chem.* **1977,** *16*, 1021.
30. Barandiaran, Z.; Seijo, L., Structure and Spectroscopy of U^{4+} Defects in Cs_2ZrCl_6: Ab initio Theoretical Studies on the $5f^2$ and $5f^16d^1$ Manifolds. *J. Chem. Phys.* **2003,** *118*, 7439-7456.
31. Ordejon, B.; Seijo, L.; Barandiaran, Z., 5f-->5f Transitions of U^{4+} Ions in High-Field, Octahedral Fluoride Coordination: the Cs_2GeF_6:U^{4+} Crystal. *J. Chem. Phys.* **2005,** *123*, 204502.
32. Minasian, S. G.; Keith, J. M.; Batista, E. R.; Boland, K. S.; Clark, D. L.; Conradson, S. D.; Kozimor, S. A.; Martin, R. L.; Schwarz, D. E.; Shuh, D. K.; Wagner, G. L.; Wilkerson, M. P.; Wolfsberg, L. E.; Yang, P., Determining Relative f and d Orbital Contributions to M–Cl Covalency in MCl_6^{2-} (M = Ti, Zr, Hf, U) and $UOCl_5^-$ Using Cl K-Edge X-ray Absorption Spectroscopy and Time-Dependent Density Functional Theory. *J. Am. Chem. Soc* **2012,** *134*, 5586-5597.
33. Su, J.; Batista, E. R.; Boland, K. S.; Bone, S. E.; Bradley, J. A.; Cary, S. K.; Clark, D. L.; Conradson, S. D.; Ditter, A. S.; Kaltsoyannis, N.; Keith, J. M.; Kerridge, A.; Kozimor, S. A.; Löble, M. W.; Martin, R. L.; Minasian, S. G.; Mocko, V.; La Pierre, H. S.; Seidler, G. T.; Shuh, D. K.; Wilkerson, M. P.; Wolfsberg, L. E.; Yang, P., Energy-Degeneracy-Driven Covalency in Actinide Bonding. *J. Am. Chem. Soc* **2018,** *140*, 17977-17984.
34. Beekmeyer, R.; Kerridge, A., Assessing Covalency in Cerium and Uranium Hexachlorides: A Correlated Wavefunction and Density Functional Theory Study. *Inorganics* **2015,** *3*.
35. Jung, J.; Atanasov, M.; Neese, F., Ab Initio Ligand-Field Theory Analysis and Covalency Trends in Actinide and Lanthanide Free Ions and Octahedral Complexes. *Inorg. Chem.* **2017,** *56*, 8802-8816.
36. Eisenstein, J. C.; Pryce, M. H. L., Interpretation of the Solution Absorption Spectra of the $(PuO_2)^{++}$ and $(NpO_2)^+$ Ions. *J. Res. Nat. Bur. Stand. Sect. A.* **1966,** *70A*, 165.

37. Edelstein, N. M., Reanalysis of the Aqueous Spectrum of the Neptunyl(V) [NpO_2^+] Ion. *J. Phys. Chem. A* **2015,** *119*, 11146-11153.
38. Lohr, L. L., Optical Spectra of Divalent Manganese Salts. I. Energy Levels for Cubic and Lower-Symmetry Complexes. *J. Chem. Phys.* **1966,** *45*, 3611-3622.
39. Wybourne, B. G., *Spectroscopic Properties of Rare Earths*. Interscience Publishers: New York, 1965.
40. Judd, B. R., *Operator Techniques in Atomic Spectroscopy*. McGraw-Hill: New York, 1963.
41. Condon, E. U., Shortley, G. H., *The Theory of Atomic Spectra*. Cambridge: 1935.
42. Van Deurzen, C. H. H.; Rajnak, K.; Conway, J. G., Uranium Five (UV), The $^1S_0$ Level and a Parametric Analysis in the $5f^2$ Configuration. *J. Opt. Soc. Am. B* **1984,** *1*, 45.
43. Martin, W. C.; Zalubas, R.; Hagan, L., *Atomic Energy Levels-The Rare-Earth Elements*. U.S. Government Printing Office: 1978.
44. Wyart, J. F.; Meftah, A.; Sinzelle, J.; Tchang-Brillet, W. U. L.; Spector, N.; Judd, B. R., Theoretical Study of Ground-State Configurations 4f(N) in NdIV, PrIV and NdV. *J. Phys. B-At. Mol. Opt. Phys.* **2008,** *41*, 085001.
45. Tanner, P. A., Spectra, Energy Levels, and Energy Transfer in High Symmetry Lanthanide Compounds. *Top. Curr. Chem.* **2004,** *241*, 167-278.
46. Satten, R. A.; Margolis, J. S., f^2 Configuration in a Crystalline Field. *J. Chem. Phys.* **1960,** *32*, 573.
47. Misetich, A. A.; Buch, T., Gyromagnetic Factors and Spin—Orbit Coupling in Ligand Field Theory. *J. Chem. Phys.* **1964,** *41*, 2524-2529.
48. Neese, F.; Solomon, E. I., Calculation of Zero-Field Splittings, g-Values, and the Relativistic Nephelauxetic Effect in Transition Metal Complexes. Application to High-Spin Ferric Complexes. *Inorg. Chem.* **1998,** *37*, 6568-6582.
49. Aravena, D.; Atanasov, M.; Neese, F., Periodic Trends in Lanthanide Compounds through the Eyes of Multireference ab Initio Theory. *Inorg. Chem.* **2016,** *55*, 4457-4469.
50. Atanasov, M.; Daul, C.; Güdel, H. U.; Wesolowski, T. A.; Zbiri, M., Ground States, Excited States, and Metal−Ligand Bonding in Rare Earth Hexachloro Complexes: A DFT-Based Ligand Field Study. *Inorg. Chem.* **2005,** *44*, 2954-2963.
51. Wolfsberg, M.; Helmholz, L., The Spectra and Electronic Structure of the Tetrahedral Ions MnO_4^-, CrO_4^{2-}, and ClO_4^-. *J. Chem. Phys.* **1952,** *20*, 837-843.
52. Burdett, J. K., The .sigma. Strength of Ligands Coordinated to Transition Metal Ions. *J. Am. Chem. Soc* **1979,** *101*, 580-583.
53. Lau, K. H.; Hildenbrand, D. L., Thermochemistry of the Gaseous Uranium Bromides UBr through UBr_5. *J. Chem. Phys.* **1987,** *86*, 2949-2954.
54. Dyke, J. M.; Fayad, N. K.; Morris, A.; Trickle, I. R.; Allen, G. C., A Study of the Electronic Structure of the Actinide Tetrahalides UF_4, ThF_4, UCl_4 and $ThCl_4$ Using Vacuum Ultraviolet Photoelectron Spectroscopy and SCF-Xα Scattered Wave Calculations. *J. Chem. Phys.* **1980,** *72*, 3822-3827.
55. Johnson, D. A.; Nelson, P. G., Lanthanide Ionization Energies and the Sub-Shell Break. Part 2. The Third and Fourth Ionization Energies. *J. Phys. Chem. Ref. Dat.* **2017,** *46*, 013109.
56. Coreno, M.; de Simone, M.; Green, J. C.; Kaltsoyannis, N.; Coates, R.; Hunston, C.; Narband, N.; Sella, A., Variable Photon Energy Photoelectron Spectroscopy of tris-Cyclopentadienyl Lanthanides. *Dalton Trans.* **2014,** *43*, 5134-5141.

57. Lee, E. P. F.; Potts, A. W.; Bloor, J. E., HeI and HeII Photoelectron Spectra of Lanthanide Trichlorides in the Vapour Phase. *Proc R. Soc. Series A, Math. and Phys. Sci.* **1982,** *381*, 373-393.
58. Notter, F.-P.; Bolvin, H., Optical and Magnetic Properties of the $5f^1AnX_6^{q-}$ Series: A Theoretical Study. *J. Chem. Phys.* **2009,** *130*, 184310.
59. Heit, Y. N.; Gendron, F.; Autschbach, J., Calculation of Dipole-Forbidden 5f Absorption Spectra of Uranium(V) Hexa-Halide Complexes. *J. Phys. Chem. Lett.* **2018,** *9*, 887-894.
60. Kaltsoyannis, N.; Bursten, B. E., Electronic Structure of f^1 Actinide Complexes. 1. Nonrelativistic and Relativistic Calculations of the Optical Transition Energies of AnX_6^{q-} Complexes. *Inorg. Chem.* **1995,** *34*, 2735-2744.
61. Ganyushin, D.; Neese, F., A Fully Variational Spin-Orbit Coupled Complete Active Space Self-Consistent Field Approach: Application to Electron Paramagnetic Resonance g-Tensors. *J. Chem. Phys.* **2013,** *138*, 104113.
62. Mironov, V. S.; Rosov, S. P., Semiempirical Crystal Field Calculations for f^N-Systems. II. Crystal Field Effects in Hexahalogenide PaX, UX, and UCl Complexes and in UCl_4 Crystal. *Phys. Status Solidi B* **1992,** *170*, 199-209.

TOC Graphic

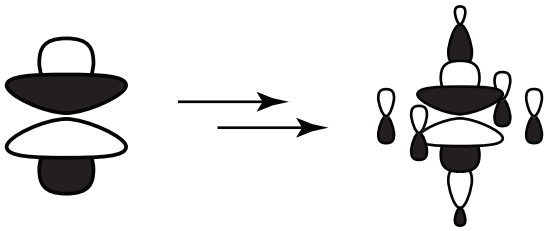

Towards ligand field theory for actinides